Journal of The Electrochemical Society, **160** (9) F910-F915 (2013)
0013-4651/2013/160(9)/F910/6/$31.00 © The Electrochemical Society

Highly Active Graphene Nanosheets Prepared via Extremely Rapid Heating as Efficient Zinc-Air Battery Electrode Material

Dong Un Lee,[a] Hey Woong Park,[a] Drew Higgins,[a,*] Linda Nazar,[b] and Zhongwei Chen[a,z]

[a]*Department of Chemical Engineering, Waterloo Institute for Nanotechnology, Waterloo Institute for Sustainable Energy, University of Waterloo, Waterloo, Ontario N2L 3G1, Canada*
[b]*Department of Chemistry, Waterloo Institute for Nanotechnology, University of Waterloo, Waterloo, Ontario N2L 3G1, Canada*

A facile method has been developed based on extremely rapid heating (temperature ramp greater than 150°C sec^{-1}) for the synthesis of graphene nanosheets with heterogeneously doped nitrogen atoms (ex-NG) in a one-step process. The nanosheets are uniquely characterized by large expansions and openings between the layers that facilitate in the diffusion of the electrolyte to perform highly active oxygen reduction reaction (ORR). Electron microscopy has verified a voile-like morphology of thermally reduced ex-NG, and X-ray photoelectron spectroscopy has confirmed successful ammonia treatment of nitrogen incorporation into the graphitic network. The ORR activity of the graphene nanosheets is evaluated using both half-cell and single-cell performance tests. The half-cell test is conducted by rotating disk electrode measurements where the nanosheets have showed very comparable ORR activity to that of state-of-the-art commercial Pt/C catalyst. A practical zinc-air battery have been utilized to test the single-cell performance of ex-NG1100, which have exhibited superior battery discharge voltages and reduced charge transfer resistance during the ORR compared to that of Pt/C. This outstanding catalytic activity of metal-free carbon-based graphene nanosheets is attributed to the opened structured attained by facile synthesis technique utilizing a rapid heating process.
 [DOI: 10.1149/2.016309jes]

Manuscript submitted April 29, 2013; revised manuscript received May 30, 2013. Published June 11, 2013.

Electric vehicles (EV) and hybrid electric vehicles (HEV) are of growing interest as technologies to minimize urban pollution, decrease petroleum demand, and potentially lower CO_2 emissions. For vehicular transport, metal-air batteries are potentially viable energy storage systems for "range extension" due to much higher theoretical energy densities than the current state-of-the-art lithium-ion batteries.[1] However, one hurdle is the development of a highly active electrocatalyst to facilitate efficient oxygen reduction reaction (ORR) at the battery's air-breathing electrode. Until recently, highly efficient ORR in aqueous media has been made possible by the use of carbon supported precious metal-based electrocatalysts such as platinum and palladium.[2–6] Even so, the kinetics of ORR is still sluggish, and the electrochemical stability is poor over long periods of operation.[7,8] In addition, the high cost of precious metals due to their global scarcity makes commercialization of devices using these materials less viable. To overcome these shortcomings, intense research efforts have been put into the development of alternative, inexpensive cathode electrocatalysts that exhibit a high activity for ORR.[9–14] Graphene, with its intriguing properties such as large surface area, high electrical conductivity, and thermal and chemical stability, has recently received enormous attention as a possible candidate.[11,15–17] Especially nitrogen-doped graphene has been found to have outstanding electrochemical activity toward ORR,[18–20] providing affordable means as a metal-free carbon-based catalyst to be used as an electrode material for fuel-cells and metal-air batteries.

Previously, various synthetic routes to prepare nitrogen-doped graphene have been reported;[21,22] however, they are often expensive and complex to set up, and large scale production is difficult for practical applications. In addition, most commonly used chemical vapor deposition (CVD) for graphene synthesis requires metal substrates such as nickel or copper as the growth catalyst/substrate. In early works of thermally reduced graphene oxide (GO), only accordion or worm-like morphologies had been demonstrated with far less degree of expansion of the graphitic layers.[23,24] Later in the journal of Chemistry of Materials, a well-known report was published on the investigation of the heating rate (maximum of 50°C min^{-1}), but also exhibited graphene sheets that were observed to be rather densely packed.[25]

In this report, our motivation is then to utilize extremely rapid heating rate for the synthesis of highly open structured graphene sheets with doped heterogeneous nitrogen species (ex-NG) in a one-step process, and achieve high electrocatalytic activity for oxygen reduction reaction (ORR). This one-step technique strategically combines two separate processes of thermal reduction and ammonia treatment to produce large batches of graphene nanosheets without the use of a substrate or metallic catalyst layer. The morphological change of the sheets occurs due to the extremely rapid evolution of the gases formed during the decomposition of the oxygen groups of GO, resulting in expansion faster than the GO sheets can knit together *via* van der Waals bonding.[25] However, to prevent the slow diffusion of the evolved gases that occurs during traditional heating processes - which leads to a more gentle reduction process - we apply extremely rapid heating rate by exposing GO from room temperature to temperatures greater than 800°C within five seconds, creating temperature rates of 150°C sec^{-1} or greater. This triggers the escape of most of the evolved gases in a very short period of time, and maximizes the expansion of the graphene sheets. Hence, with the ability to control the morphology via our facile and robust synthesis technique, we have designed and produced graphene nanosheets with highly efficient ORR activity, which have been confirmed by both half-cell and single-cell performance testing.

Experimental

Graphene oxide (GO) synthesis.— GO is synthesized from natural graphite flakes by the modified Hummers' method.[26] In a typical GO preparation, 2 g of graphite powder (Alfa Aesar) is stirred in 46 mL of concentrated sulphuric acid (Fisher Scientific) for 10 hours. The mixture is put into an ice bath and 1 g of sodium nitrate (Aldrich) is added followed by the addition of 6 g of potassium permanganate (EMD) under stirring. The mixture is removed from the ice bath and stirred for 1 hour. Then 92 mL of distilled de-ionized (DDI) water is added drop-wise and stirred for another 30 minutes followed by the addition of 280 mL of warm DDI water (40°C) and 40 mL of 30% H_2O_2 (Fisher Scientific). The mixture is filtered and washed with 3 L of 5% HCl solution, then centrifuged five times at 4000 rpm for 10 min. The product is collected and dried in room temperature.

One-step thermal reduction and ammonia treatment under extreme heating rate.— In a typical one-step rapid heating synthesis, the quartz tube is vacuumed and filled with Ar (Praxair) three times, and 100 mg of GO is loaded outside of the heating zone of the horizontal tube furnace. Under 100 sccm of Ar protection, the furnace is heated to a desired temperature after which 50 sccm of NH_3 (Praxair) is introduced to the tube and Ar flow is reduced to 50 sccm. Ar/NH_3 mixture is allowed to flow for five minutes then the position of the quartz tube is shifted along the horizontal furnace in less than 5 seconds to quickly

*Electrochemical Society Student Member.
[z]E-mail: zhwchen@uwaterloo.ca

bring GO to the heating zone in the center of the furnace. This rapid increase in temperature allows the sheets of GO to thermally reduce and expand, while the Ar/NH_3 flow allows nitrogen-doping, in a one-step process. At this point, we have exfoliated and nitrogen-doped graphene nanosheets (ex-NG). The sample names are referred as ex-NG800, ex-NG900, ex-NG1000, and ex-NG1100 based on the temperature at which the synthesis is carried out (800°C, 900°C, 1000°C, and 1100°C, respectively). After 10 minutes of NH_3 treatment, the tube is shifted back to bring the sample to the outside of the heating zone. The furnace is cooled down under 100 sccm of Ar protection then the sample is collected from the quartz boat for direct use.

Material characterization.— Scanning electron microscopy (SEM) (LEO FESEM 1530) and transmission electron microscopy (TEM) (Philips CM300) are utilized to observe the surface morphology and structure of the graphene nanosheets, while high-resolution TEM (HRTEM) and selected area electron diffraction (SAED) are used to study the crystallinity. X-ray diffraction (XRD) (AXS D8 Advance, Brunker) is used to investigate the change in 002 peak angle of the graphene nanosheets after the one-step synthesis, and Raman spectroscopy (LabRAM HR, HORIBA scientific) is used to study the change in the graphitic bonds. X-ray photoelectron spectroscopy (XPS) (K-Alpha XPS spectrometer, Thermal Scientific) is conducted to determine the atomic composition of the graphene nanosheets and to quantify nitrogen content of different species.

Three-electrode half-cell test.— The ORR activity of ex-NG in the aqueous electrolyte (0.1 M KOH) is tested in a three-electrode electrochemical cell using rotating disk electrode (RDE) voltammetry, which consists of a potentiostat (Pine Instrument Co., AFCBP-1), a rotation speed controller (Pine Instrument Co., AFMSRCE). All RDE voltammetry are performed at room temperature using a Saturated Calomel Electrode (SCE) as a reference electrode. A platinum wire is used as the counter electrode. A glassy carbon electrode (5 mm OD) coated with 20 uL of 4 mg mL^{-1} ex-NG suspension made by mixing ex-NG and a solution of 0.5 wt% Nafion in ethanol is used as the working electrode (catalytic loading of ca. 0.4 mg cm^{-2}). Similarly, 20 wt% Pt/C coated working electrode is prepared on a glassy carbon with the same loading as a comparison. ORR curves are recorded from −1.0 to 0.2 V at a scan rate of 10 mV s^{-1} with O_2-saturated electrolyte under various electrode rotation speeds (100, 400, 900, 1600 rpm). The ORR polarization curves are background corrected by subtracting the currents obtained under the same testing conditions in Ar-electrolyte.

Zinc-air practical single-cell test.— The single-cell ORR activity of ex-NG is tested using a home-made practical zinc-air battery and a multichannel potentiostat (Princeton Applied Research, VersaSTAT MC). A polished zinc plate (Zinc Sheet EN 988, OnlineMetals) and a catalyst-coated gas diffusion layer (Toray Carbon Paper TGP-H-120, FuelCellStore) are used as the anode and cathode, respectively. Microporous membrane (25 μm polypropylene membrane, Celgard 5550) and stainless steel mesh are used as a separator and current collectors, respectively. 6 M KOH is used as the electrolyte. The area of the gas diffusion layer exposed to the electrolyte is 2.84 cm^2. All active materials (ex-NG1100 and 20 wt% Pt/C) are sprayed-coated using an air brush onto the gas diffusion layer with a loading of ca. 0.7 mg cm^{-2}. Briefly, 9.4 mg of active material is dispersed in 1 mL of isopropyl alcohol by sonication for 30 minutes. Then 67 μL of 5 wt% Nafion solution is added followed by 1 hour of additional sonication. The catalyst mixture is sprayed onto the gas diffusion layer then dried in an oven at 80°C for 1 hour. The catalyst loading is determined by measuring the weight of the gas diffusion layer before and after spray coating. The discharge polarization and power density plots are obtained by a galvanodynamic method with a current density ranging from 0 to 70.7 mA cm^{-2}. Electrochemical impedance spectroscopy (EIS) is conducted with a direct current (DC) voltage fixed at an ORR potential of 0.8 V with an alternating current (AC) voltage of 20 mV ranging from 100 kHz to 0.1 Hz to obtain Nyquist plots.

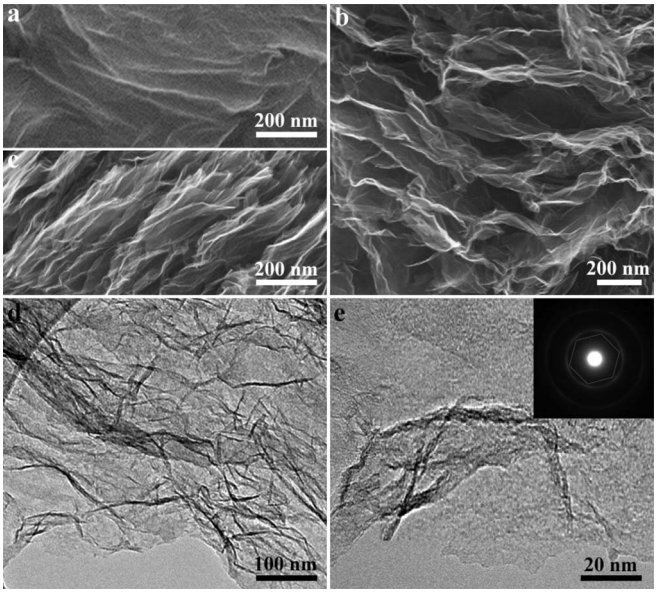

Figure 1. SEM images of (a) GO prior to one-step thermal reduction and ammonia treatment, (b) ex-NG1100-S synthesized by slow heating ramp (5°C min^{-1}), and (c) ex-NG1100 synthesized by extremely rapid heating ramp (∼150°C sec^{-1}). A typical TEM image of ex-NG1100 with randomly oriented wrinkles and folds. (d) HRTEM image of ex-NG1100 (Inset: SAED pattern of a few layers of ex-NG1100).

Results and Discussion

After the one-step thermal reduction and ammonia treatment under an extreme heating rate, the morphological change from GO to ex-NG synthesized at 1100°C (ex-NG1100) is revealed by SEM analysis. The layered structure observed with GO (Figure 1a) has been clearly converted into voile-like sheets of graphene (Figure 1b), indicative of successful thermal reduction of oxygen groups of GO.[21,24] The large expansions and openings observed between the graphene nanosheets is most likely due to the very rapid heating process, which have allowed the discharge of evolved gases from GO to occur with much higher kinetic energy, thereby expanding the sheets. Compared to previous reports on thermal reduction of GO, which exhibit accordion or worm-like morphologies,[23–25] the unique open-structured morphology with large interlayer spacing presented in this study is highly suitable for the electrocatalysis of oxygen reduction, as we demonstrate its enhanced performance in the later sections by both half-cell and single-cell testing. The wrinkles observed in the graphene nanosheets are most likely due to the incorporation of heterogeneous nitrogen species into the graphitic network, which may prevent restacking of the sheets. In order to experimentally verify the effect of heating rate on the degree of expansion of the graphene nanosheets and its electrochemical performance, ex-NG1100-S have been synthesized by very slow heating rate of 5°C min^{-1} (compared to ∼200°C sec^{-1} for ex-NG1100) (Figure 1c). The SEM analysis clearly shows much densely packed morphology compared to that of ex-NG1100, most probably due to the discharge gases having insufficient energy to expand the sheets. TEM characterization also confirms wrinkled surfaces of ex-NG1100 (Figure 1d), similar to those observed in the SEM characterization.[20] HRTEM, on the other hand, reveals wavy edges of the graphene sheets, which is probably due to the ammonia in the feedstock more readily reacting with the edge planes to incorporate heterogeneous nitrogen species (Figure 1e). The basal planes are observed to have maintained the integrity of the graphitic network as no perforation or defects are observed in the sheets. This

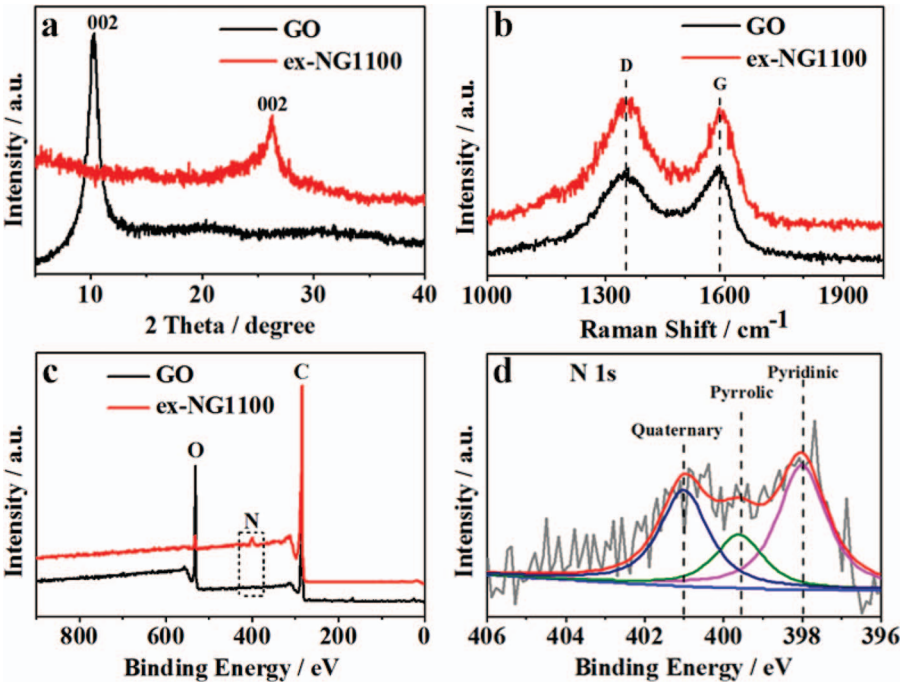

Figure 2. (a) XRD patterns of GO and ex-NG1100. (b) Raman spectra of GO and ex-NG1100. (c) Full XPS spectra of GO and ex-NG1100. (d) High-resolution N 1s XPS spectrum of ex-NG1100. (The gray line is the original signal, and the red curve is the result of the curve fit. Blue, green, and pink peaks correspond to quaternary, pyrrolic, and pyridinic nitrogen species, respectively, after de-convolution.).

is important as these surfaces facilitate the transport of charges and diffusion of reactants during catalysis of ORR. To corroborate, the inset of Figure 1e shows the selected area electron diffraction (SAED) pattern from a few layers of ex-NG1100 with a hexagonal symmetry, which is characteristic of the symmetrical three-fold sp^2 bonding of carbon atoms.[27] This again confirms that the graphitic network is well-maintained even after ammonia treatment at 1100°C.[18,28]

The change in the structure from GO to ex-NG1100 is further quantified by the X-ray diffraction (XRD) pattern (Figure 2a). The 002 reflection assigned to the layer-to-layer distance in the graphitic structures of GO at 10.3° in 2θ shifts from a d-spacing of 8.57 Å to a much lower value of 3.50 Å for ex-NG1100 (25.4° in 2θ), due to the departure of the oxygen groups of GO upon thermal reduction.[25] The degree of structural deformation incurred by thermal reduction and ammonia treatment is verified by comparing the Raman shifts of GO and ex-NG1100 (Figure 2b). Two peaks are observed in both spectra, at approximately 1350 cm^{-1} and 1590 cm^{-1}, corresponding to the D and G bands, respectively. The D band is characteristic of disorder in the structure caused by defects within the graphitic plane, while the G band is characteristic of the sp^2 bonds within any graphitic material which has E_{2g} vibrational modes. The ratio of the intensities of the two bands, I_D/I_G, thus reflects the fraction of structural defects and degree of exposure of the edge planes. A higher I_D/I_G ratio of 1.14 is observed with ex-NG1100 compared to that of 0.97 with GO, consistent with previously reported work.[29] This suggests successful one-step thermal reduction and nitrogen-doping of ex-NG because the expansion of the graphene sheets and the incorporation of the heterogeneous nitrogen species into the graphitic structure have resulted in increased edge plane exposure and creation of defects.[30] From the analysis of X-ray photoelectron spectroscopy (XPS), a characteristic peak corresponding to the presence of nitrogen species is observed in the spectrum of ex-NG1100, which is absent in that of GO, confirming successful doping of nitrogen species (Figure 2c). The large oxygen peak is observed in the spectrum of GO due to the oxygen groups formed during the Hummers' method, while a much smaller oxygen peak in the spectrum of ex-NG1100 is indicative of reduced oxygen content due to the thermal reduction during the synthesis. The high-resolution N1s spectrum of ex-NG1100 reveals the atomic percent of nitrogen to be ca. 3.5%, with a distribution of nitrogen into three species: pyridinic N, pyrrolic N, and quaternary N, based on spectral de-convolution (Figure 2d).[31,32] As the synthesis temperature of ex-NG is increased, the nitrogen content decreases due to the decomposition of the nitrogen species at higher temperatures, consistent with previous reports (Table I).[14,20]

To investigate the effect of synthesis temperature on the morphology of the graphene nanosheets, graphene nanosheets have been prepared at temperatures 800, 900, 1000, and 1100°C. A trend is clearly observed from the SEM analysis where the increase in the synthesis temperature increases the degree of wrinkling and the degree of expansion of the sheets (Figure 3a, 3b, 3c, and 3d). This is again most probably caused by more energetic release of the gases from the graphene sheets during the thermal reduction at elevated temperatures. Hence, the synthesis temperature has effect on not only the final composition but also the morphology of the graphene nanosheets both of which can be easily controlled by this synthesis technique. This highlights the practical feasibility of effectively designing a catalyst with correct composition and morphology to obtain highly active ORR catalyst.

To elucidate the effect of heating rate used during the synthesis on the ORR activity of the graphene nanosheets, RDE measurements have been performed with ex-NG1100-S and compared to that of ex-NG1100 (Figure 4a). With more negative onset potential, which is indicative of larger ORR overpotential, ex-NG1100-S is observed to perform poorly, exhibiting lower magnitude of current densities at all points in the potential window tested compared to ex-NG1100. Even though a slight variation in the nitrogen content may exist between the two types of graphene nanosheets due to different heating rates, the superior performance of ex-NG1100 is most likely ascribed to its open structure as confirmed by the SEM analysis, which allows

Table I. Atomic percent nitrogen content and its distribution into different nitrogen species obtained from de-convolution of the N1s XPS peaks. The numbers in brackets indicate the percentage of the nitrogen species in the three species.

Sample	N content, at%	pyridinic N, at%	pyrrolic N, at%	quaternary N, at%
ex-NG800	5.80	3.10 (53.5%)	1.32 (22.8%)	1.37 (23.7%)
ex-NG900	5.44	2.98 (54.8%)	1.14 (20.9%)	1.32 (24.2%)
ex-NG1000	5.18	2.58 (49.9%)	1.23 (23.8%)	1.36 (26.3%)
ex-NG1100	3.50	1.59 (45.4%)	0.69 (19.6%)	1.22 (35.0%)

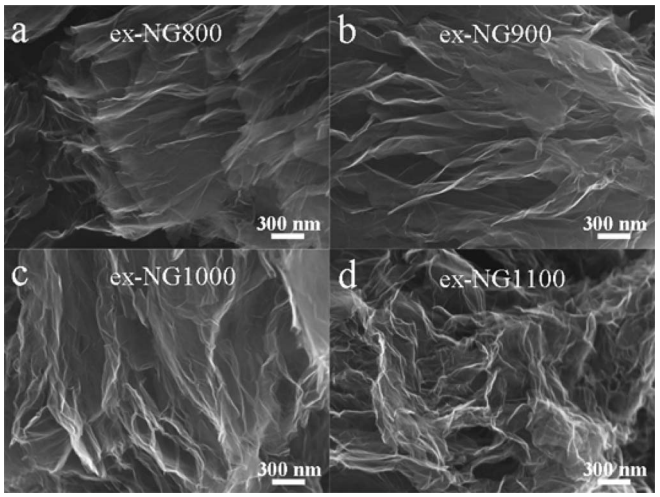

Figure 3. SEM images of ex-NG synthesized by one-step thermal reduction and nitrogen-doping at various temperatures of (a) 800°C, (b) 900°C, (c) 1000°C, and (d) 1100°C.

better diffusion of the electrolyte for highly efficient ORR activity. The RDE measurements of the graphene sheets produced at different temperatures have also been conducted to study the effect of synthesis temperature on the ORR activity (Figure 4b). As expected, the graphene nanosheets show improvement in both the onset and half-wave potentials, and larger observed current densities as the synthesis temperature is increased. As discussed in Figure 3, this trend is ascribed to higher degrees of expansion of the graphene sheets at higher temperatures providing the best morphology for highly efficient ORR activity. Furthermore, since the heterogeneous nitrogen atoms incorporate into the graphene sheets as "defects", larger nitrogen contents at lower temperatures disrupt the graphitic network, which likely have been detrimental to the ORR performance. Also, graphitization of the carbon atoms during the synthesis may play an important role in governing the ORR activity as it may be related to electrical properties. At high temperatures, especially for ex-NG1100, the graphitization has probably occurred more readily due to higher kinetics. Combined with a moderate amount of heterogeneously doped nitrogen atoms from the ammonia treatment, ex-NG1100 likely formed highly efficient active sites for ORR without losing electrical conductivity, resulting in best ORR performance. The kinetics study of ORR of ex-NG1100 is investigated by obtaining polarization curves at various rotation rates (Figure 4c). The Koutechý-Levich (K-L) plot drawn based on polarization curves of ex-NG1100 shows parallel lines that correspond to different potentials, which is indicative of first-order kinetics of ex-NG1100 (Figure 4d). The quantitative analysis of K-L plot has been carried out as the following. The observed current density (j) is related to the kinetic current (j_k) and limiting current density (j_L) by,

$$\frac{1}{j} = \frac{1}{j_K} + \frac{1}{j_L}$$

Then the number of electrons transferred per O_2 molecule, n, is calculated using the K-L equation,

$$j_L = 0.2nFD_O^{2/3}\upsilon^{-1/6}C_O\omega^{1/2}$$

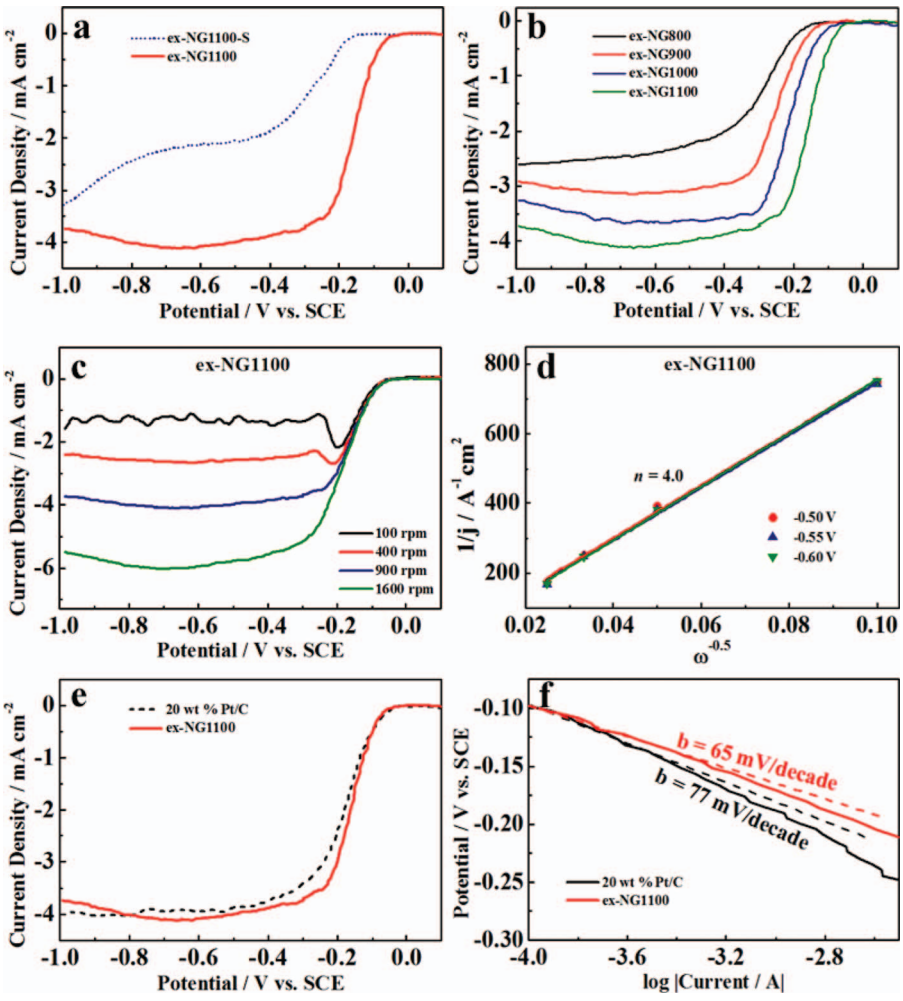

Figure 4. ORR polarization curves of (a) ex-NG1100-S and ex-NG1100, and (b) ex-NG800, ex-NG900, ex-NG1000 and ex-NG1100 obtained at 900 rpm in 0.1 M KOH. (c) RDE measurements of ex-NG1100 obtained at rotation rates of 100, 400, 900, and 1600 rpm. (d) Koutecký-Levich (K-L) plot of ex-NG1100 obtained at potentials −0.50, −0.55, and −0.60 V vs. SCE. (e) ORR polarization curves of Pt/C and ex-NG1100 obtained at 900 rpm. (f) Tafel plot of Pt/C and ex-NG1100 at the high potential region.

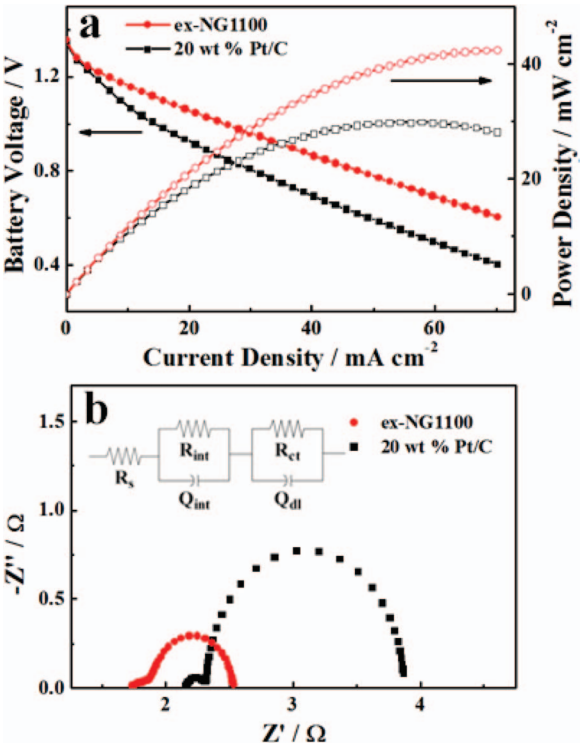

Figure 5. Zinc-air single-cell battery performance of (a) galvanodynamic discharge and corresponding power density curves of Pt/C and ex-NG1100, and (b) Nyquist plot obtained by EIS of Pt/C and ex-NG1100 air electrodes.

In the above equation, j_L is the limiting current density, F is the Faraday constant (96 485 C mol^{-1}), D_o is the diffusion coefficient of O_2 (1.9×10^{-5} cm^2 s^{-1}) in 0.1 M KOH, υ is the kinematic viscosity of 0.1 M KOH (0.01 cm^2 s^{-1}), and C_o is the concentration of O_2 in the electrolyte (1.1×10^{-6} mol cm^{-3}).[33] At the ORR potentials of −0.50 V, −0.55 V, and −0.60 V (vs. SCE), the determined value of *n* is 4.0, which is an indication of highly efficient electrochemical reduction of O_2 occurring via a pseudo four-electron reduction pathway ($O_2 + 2H_2O + 4e^- \rightarrow 4OH^-$). Typically, ORR that occurs on carbon electrodes involves less than 4 electrons, but there also have been reports that up to 4 electron reduction pathways take place on nitrogen-containing carbon electrodes.[34–36] The practical viability is demonstrated by comparing the excellent ORR activity of ex-NG1100 to that of state-of-the-art commercial carbon supported 20 wt% platinum (Pt/C) catalyst (Figure 4e). The onset and half-wave potentials of −0.050 V (vs. SCE) and −0.164 V (vs. SCE), respectively, are demonstrated by ex-NG1100, which are very comparable to those of Pt/C (−0.039 V and −0.179 V (vs. SCE), respectively). Furthermore, the analysis of the Tafel plot have resulted in a shallower slope of 65 mV/decade for ex-NG1100 compared to that of Pt/C (77 mV/decade), which is indicative of superior ORR kinetics of ex-NG1100 in the high overpotential regime (Figure 4f). This outstanding ORR performance of metal-free carbon-based ex-NG1100 electrocatalyst with precisely tailored morphology has been possible with a well-controlled facile synthesis technique.

To demonstrate the feasibility of commercialization of the graphene nanosheets, a home-made zinc-air battery is used to evaluate the single-cell performance of the catalyst in the realistic conditions. The galvanodynamic discharge curves of ex-NG1100 and Pt/C show a typical profile with initial voltage drop due to the activation followed by pseudolinear voltage drop due to the ohmic losses (Figure 5a). In comparison, the discharge voltages of ex-NG1100 at all points of the current densities measured are significantly higher than those of Pt/C. Furthermore, single-cell current density of ex-NG1100 (47.6 mA cm^{-2}) at 0.8 V discharge voltage is over 1.5 times than that of Pt/C (30.5 mA cm^{-2}). This superior performance of ex-NG1100 is attributed its unique morphology that is able to undergo much efficient ORR. In addition, significantly higher peak power density is observed with ex-NG1100 (42.4 mW cm^{-2}) compared to that of Pt/C (29.9 mW cm^{-2}). To further characterize the performance of the air electrodes, EIS have been conducted. The Nyquist plot of ex-NG1100 and Pt/C obtained at 0.8 V DC voltage have revealed resistances associated with the electrical conductivity of the air electrodes as well as the charge transfer process during ORR (Figure 5b). The impedance spectra of both ex-NG1100 and Pt/C show a small semicircle in the high frequency region followed by a larger semicircle in the mid to low frequencies. This type of impedance behavior is well described by an equivalent circuit shown in the inset of Figure 5b with five elements, R_s, Q_{int}, R_{int}, Q_{dl}, and R_{ct}.[13,37] The value of R_s is representative of the internal resistance including the resistance arising from the electrolyte, electrocatalyst and contact resistances. R_{int} is characteristic of the solid liquid interface resistance, and R_{ct} is strongly related to the resistance that arises from the charge transfer process during ORR. The constant phase elements Q_{int} and Q_{dl} are added in the equivalent circuit to represent the capacitances that arise from the solid electrolyte interface of the air electrode.[13,37] The values of these five elements for both ex-NG1100 and Pt/C are summarized in Table II. A slightly higher R_{int} observed for ex-NG1100 (0.357 Ω) than with Pt/C (0.186 Ω) can be ascribed to the resistances that arises from hydrophobic surface of the graphene nanosheets in contact with the aqueous electrolyte. Nonetheless, R_{ct} obtained for ex-NG1100 (0.550 Ω) is almost 3 times smaller than that of Pt/C (1.55 Ω), which is a strong evidence that the electrical resistance of the charge transfer process have been significantly reduced during ORR for ex-NG1100. This bolsters our earlier speculation that better graphitization at higher synthesis temperatures contributes in improving the ORR activity. The outstanding single-cell performance of ex-NG1100 is attributed to its high ORR activity due to morphological advantages as well as excellent electric properties attained by the graphene nanosheets that facilitate in the charge transfer process during ORR catalysis.

Table II. Values of the five elements from EIS analysis of ex-NG1100 and 20 wt% Pt/C.

Element	ex-NG1100	20 wt% Pt/C
R_s (Ω)	1.70	2.14
R_{int} (Ω)	0.357	0.186
R_{ct} (Ω)	0.550	1.55
Q_{int} ($S \cdot s^n$)	5.60	7.05×10^{-3}
Q_{dl} ($S \cdot s^n$)	0.0847×10^{-2}	5.68×10^{-2}

Conclusions

In summary, we show that by our one-step synthesis technique that utilizes a rapid heating rate, thermally reduced and nitrogen-doped graphene sheets with well-controlled morphology can be produced to exhibit highly active ORR performance. In a half-cell testing, ex-NG have shown comparable ORR activity to that of state-of-the-art 20 wt% Pt/C catalyst. In a single-cell testing using a practical zinc-air battery, ex-NG outperformed with superior battery discharge voltages and significantly smaller charge transfer resistances during ORR. This outstanding catalytic performance of metal-free carbon-based graphene nanosheets is a promising candidate for commercialization as a highly efficient electrode material for fuel cells and metal-air batteries.

Acknowledgment

This research was supported by the Natural Sciences and Engineering Research Council of Canada (NSERC) through grants to Dr. Zhongwei Chen and Dr. Linda F. Nazar, and the University of Waterloo.

References

1. G. Girishkumar, B. McCloskey, A. C. Luntz, S. Swanson, and W. Wilcke, *J. Phys. Chem. Lett.*, **1**, 2193 (2010).
2. S. Guo, S. Dong, and E. Wang, *ACS Nano*, **4**, 547 (2009).
3. J.-S. Lee, S. Tai Kim, R. Cao, N.-S. Choi, M. Liu, K. T. Lee, and J. Cho, *Adv. Energy Mater.*, **1**, 34 (2011).
4. A. Kongkanand, S. Kuwabata, G. Girishkumar, and P. Kamat, *Langmuir*, **22**, 2392 (2006).
5. Y. H. Bing, H. S. Liu, L. Zhang, D. Ghosh, and J. J. Zhang, *Chem. Soc. Rev.*, **39**, 2184 (2010).
6. D. C. Higgins, D. Meza, and Z. Chen, *J. Phys. Chem. C*, **114**, 21982 (2010).
7. K. Gong, F. Du, Z. Xia, M. Durstock, and L. Dai, *Science*, **323**, 760 (2009).
8. Y. Liang, H. Wang, J. Zhou, Y. Li, J. Wang, T. Regier, and H. Dai, *Journal of the American Chemical Society*, **134**, 3517 (2012).
9. J.-Y. Choi, D. Higgins, and Z. Chen, *Journal of the Electrochemical Society*, **159**, B87 (2012).
10. J. Wu, W. Li, D. Higgins, and Z. Chen, *J. Phys. Chem. C*, **115**, 18856 (2011).
11. Z. Chen, J.-Y. Choi, H. Wang, H. Li, and Z. Chen, *Journal of Power Sources*, **196**, 3673 (2011).
12. D. Higgins, Z. Chen, and Z. Chen, *Electrochimica Acta*, **56**, 1570 (2011).
13. Z. Chen, A. Yu, D. Higgins, H. Li, H. Wang, and Z. Chen, *Nano Letters*, **12**, 1946 (2012).
14. X. Li, H. Wang, J. T. Robinson, H. Sanchez, G. Diankov, and H. Dai, *Journal of the American Chemical Society*, **131**, 15939 (2009).
15. A. K. Geim and K. S. Novoselov, *Nature Materials*, **6**, 183 (2007).
16. S. Yang, X. Feng, X. Wang, and K. Müllen, *Angewandte Chemie International Edition*, **50**, 5339 (2011).
17. G. Yu, L. Hu, M. Vosgueritchian, H. Wang, X. Xie, J. R. McDonough, X. Cui, Y. Cui, and Z. Bao, *Nano Letters*, **11**, 2905 (2011).
18. L. Qu, Y. Liu, J.-B. Baek, and L. Dai, *ACS Nano*, **4**, 1321 (2010).
19. K. R. Lee, K. U. Lee, J. W. Lee, B. T. Ahn, and S. I. Woo, *Electrochemistry Communications*, **12**, 1052 (2010).
20. D. Geng, Y. Chen, Y. Chen, Y. Li, R. Li, X. Sun, S. Ye, and S. Knights, *Energy Environ. Sci.*, **4**, 760 (2011).
21. D. Usachov, O. Vilkov, A. Grüneis, D. Haberer, A. Fedorov, V. K. Adamchuk, A. B. Preobrajenski, P. Dudin, A. Barinov, M. Oehzelt, C. Laubschat, and D. V. Vyalikh, *Nano Letters*, **11**, 5401 (2011).
22. H. Wang, Q. Wang, Y. Cheng, K. Li, Y. Yao, Q. Zhang, C. Dong, P. Wang, U. Schwingenschlögl, W. Yang, and X. X. Zhang, *Nano Letters*, **12**, 141 (2011).
23. S. Lee, D. Cho, and L. T. Drzal, *J Mater Sci*, **40**, 231 (2005).
24. A. Celzard, J. F. Mareche, and G. Furdin, *Prog. Mater. Sci.*, **50**, 93 (2005).
25. M. J. McAllister, J.-L. Li, D. H. Adamson, H. C. Schniepp, A. A. Abdala, J. Liu, M. Herrera-Alonso, D. L. Milius, R. Car, R. K. Prud'homme, and I. A. Aksay, *Chemistry of Materials*, **19**, 4396 (2007).
26. W. S. Hummers and R. E. Offeman, *Journal of the American Chemical Society*, **80**, 1339 (1958).
27. G.-P. Dai, J.-M. Zhang, and S. Deng, *Chemical Physics Letters*, **516**, 212 (2011).
28. Z. Jin, J. Yao, C. Kittrell, and J. M. Tour, *ACS Nano*, **5**, 4112 (2011).
29. K. N. Kudin, B. Ozbas, H. C. Schniepp, R. K. Prud'homme, I. A. Aksay, and R. Car, *Nano Letters*, **8**, 36 (2007).
30. D. Geng, S. Yang, Y. Zhang, J. Yang, J. Liu, R. Li, T.-K. Sham, X. Sun, S. Ye, and S. Knights, *Applied Surface Science*, **257**, 9193 (2011).
31. F. d. r. Jaouen, J. Herranz, M. Lefèvre, J.-P. Dodelet, U. I. Kramm, I. Herrmann, P. Bogdanoff, J. Maruyama, T. Nagaoka, A. Garsuch, J. R. Dahn, T. Olson, S. Pylypenko, P. Atanassov, and E. A. Ustinov, *ACS Applied Materials & Interfaces*, **1**, 1623 (2009).
32. P. H. Matter, L. Zhang, and U. S. Ozkan, *Journal of Catalysis*, **239**, 83 (2006).
33. G. Wu, G. Cui, D. Li, P.-K. Shen, and N. Li, *Journal of Materials Chemistry*, **19**, 6581 (2009).
34. T. Iwazaki, R. Obinata, W. Sugimoto, and Y. Takasu, *Electrochemistry Communications*, **11**, 376 (2009).
35. J.-i. Ozaki, N. Kimura, T. Anahara, and A. Oya, *Carbon*, **45**, 1847 (2007).
36. R. A. Sidik, A. B. Anderson, N. P. Subramanian, S. P. Kumaraguru, and B. N. Popov, *J. Phys. Chem. B*, **110**, 1787 (2006).
37. D. Thiele and A. Züttel, *Journal of Power Sources*, **183**, 590 (2008).